Localized Iris Image Quality Using 2-D Wavelets

Yi Chen, Sarat C. Dass, and Anil K. Jain

Michigan State University, East Lansing, MI, 48823
{chenyi1, jain}@cse.msu.edu, {sdass}@stt.msu.edu

Abstract

The performance of an iris recognition system can be undermined by poor quality images and result in high false reject rates (FRR) and failure to enroll (FTE) rates. In this paper, a wavelet-based quality measure for iris images is proposed. The merit of the this approach lies in its ability to deliver good spatial adaptivity and determine local quality measures for different regions of an iris image. Our experiments demonstrate that the proposed quality index can reliably predict the matching performance of an iris recognition system. By incorporating local quality measures in the matching algorithm, we also observe a relative matching performance improvement of about 20% and 10% at the equal error rate (EER), respectively, on the CASIA and WVU iris databases.

1 Introduction

Iris recognition is considered the most reliable form of biometric technology with impressively low false accept rates (FARs), compared to other biometric modalities (e.g., fingerprint, face, hand geometry, etc) [1]. However, recent studies on iris recognition systems have reported surprisingly high false reject rates (FRRs) (e.g., 11.6% [3], 7% [4] and 6% [5]), due to poor quality images. Causes of such poor quality include occlusion, motion, poor focus, non-uniform illumination, etc. (see Figure 1(a)) [2].

There have been several efforts in iris image quality analysis in the past. Daugman [7] measured the energy of high frequency components in Fourier spectrum to determine the focus. Zhang and Salganicoff [8] analyzed the sharpness of the pupil/iris boundary for the same purpose. Ma et al. [9] proposed a quality classification scheme to categorize iris images into four classes, namely clear, defocused, blurred and occluded.

We propose a novel iris quality measure based on local regions of the iris texture. Our argument is that the iris texture is so localized that the quality varies from region to region. For example, the upper iris regions are more often occluded than lower regions, and the inner regions often provide finer texture compared to the outer regions (see Figure 1(b)). Sung et al. have shown that by simply weighting the inner (respectively, outer) iris regions with the weight $1(0)$, the matching performance can be improved [12]. To estimate the local quality, we employ 2D wavelets on concentric bands of a segmented iris texture. By weighting the matching distance using the local quality, we observe a relative improvement of about 20% and 10% at the equal error rate (EER) in the matching performance, respectively, on CASIA1.0 [16] and WVU databases. Further, we combine the local quality into a single image quality index, Q, and demonstrate its capability of predicting the matching performance.

The rest of the paper is organized as follows: Section 2 describes the iris segmentation algorithms. In Section 3, localized quality are derived using 2D wavelets. In Section 4, an overall quality index Q is computed. Two experiments are conducted in Section 5

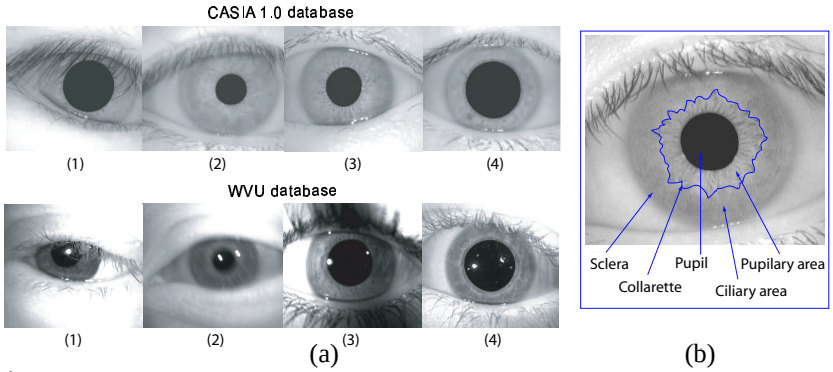

Fig. 1. (a) Poor quality of iris images caused by (1) occlusion, (2) poor focus and eye motion, (3) non-uniform illumination, and (4) large pupil area. The top (respectively, bottom) panels are images from the CASIA1.0 (WVU) databases. (b) Components of the eye and iris pattern. The inner iris (pupillary) area and the outer iris (ciliary) area are separated by the collarette boundary.

to predict and improve the matching performance using the quality derived. Summary and conclusions are provided in Section 6.

2 Image Preprocessing

The iris region, consisting of the annulus band between the pupil and sclera (see Figure 1(b)), is the essential feature used in iris biometric systems. The segmentation of iris region involves two steps, (i) iris boundary detection, and (ii) eyelid detection.

The iris/sclera boundary and the pupil/iris boundary (see Figure 1(b)) can be approximated by two circles using the following method.

1. The grayscale morphological opening is conducted on a given image to remove noise (e.g., eyelashes). Intensity thresholding is used to locate the pupil area and approximate the pupil center (c) and radius (r).
2. To approximate the pupil/iris boundary, Canny edge detection is performed onto a circular neighborhood centered at c and with radius ($r + 20$). Noise-like edges are removed and the edge map is down-sampled before circular Hough transform is applied to detect the pupil/iris boundary.
3. To detect the iris/sclera boundary, Step 2 is repeated with the neighborhood region replaced by an annulus band (of width R, say) outside the pupil/iris boundary. The edge detector is tuned to the vertical direction to minimize the influence of eyelids.

The upper and lower eyelids are oval-shaped and can be approximated by second-order parabolic arcs, as shown below:

1. The original image is decomposed into four sub bands (HH, HL, LH, LL) using Daubechies wavelets [15]. The LH image, which contains details in the vertical direction is processed through Canny edge detection. Here, the Canny edge detector is tuned to the horizontal direction to minimize the influence of eyelashes.
2. To detect the upper eyelid, edges outside the upper iris/sclera boundary neighborhood are removed. The remaining edge components that are located close to each other within a certain distance are connected.
3. The longest connected edge is selected and fit with a second-order parabolic curve
$$f(x) = ax^2 + bx + c, \tag{1}$$
where a, b, c are the parameters to be estimated. The estimation is carried out by minimizing the sum of squared error $\frac{1}{N}\sum_{i=1}^{N}(f(x_i) - y_i)^2$, where $(x_i, y_i)_{i=1,2,\ldots,N}$ represent N points on the selected edge.

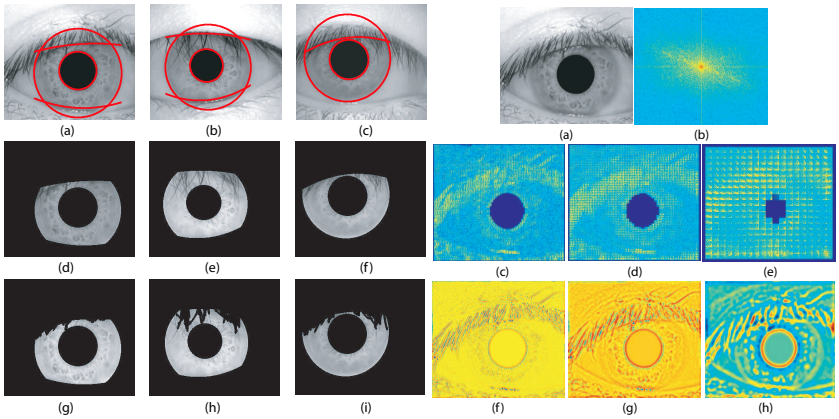

Fig. 2. (I) Three iris images from CASIA1.0 database with (a-c) iris boundaries and eyelids detected; (d-f) The extracted iris pattern; (g-i) The extracted iris pattern after eyelash removal. (II) Demonstrating the effectiveness of the wavelet transform in achieving better space-frequency localization compared to Fourier transform and STFT: (a) Original eye image; (b) Fourier transform of the image; (c-e) STFT using rectangular windows with sizes of $2 \times 4, 4 \times 6$, and 14×16, respectively; (f-h) Wavelet transform using Mexican hat with scales of $0.5, 1.0, 2.0$, respectively.

4. To detect the lower eyelid, Steps 2 and 3 are repeated with the rectangular neighborhood in Step 2 taken around the lower iris/sclera boundary.

A simple intensity thresholding operation is implemented to remove eyelashes in the CASIA1.0 database, but not in the WVU database (Note that the two databases used different iris image capture devices). Figure 2(I) illustrates the segmentation results using the algorithms discussed above on several iris images from the CASIA1.0 database.

3 Localized Quality Assessment

Ma et al. [9] used the energy of low, moderate and high frequency components in 2D Fourier power spectrum to evaluate iris image quality. However, it is well known that Fourier transform (or Short Time Fourier Transform (STFT)) does not localize in space, and is, therefore, not suited for deriving local quality measures (see Figures 2(II:b-e)). The wavelet transform, on the contrary, obtains smooth representation in both space and frequency with flexible window sizes varying up to a scale factor (see Figures 2(II:f-h)). Specifically, we use continuous wavelet transform (CWT) instead of discrete wavelet transform (DWT) so that more detailed iris features can be captured.

3.1 The Continuous Wavelet Transform (CWT)

Given an image $f(x, y) \in R^2$, its CWT, defined as the convolution with a series of wavelet functions, is given by

$$w(s, a, b) = \frac{1}{\sqrt{s}} \int \int_{R^2} f(x, y) \phi(\frac{x - a}{s}, \frac{y - b}{s}) dx dy, \tag{2}$$

where s is the dilation (scale) factor and (a, b) denotes the translation (or, shift) factor. To simplify computations, the convolution in equation (2) can be converted into multiplication in the Fourier frequency domain. For a function g, we denote by G the corresponding 2D Fourier transform of g, given by

$$G(\omega_1, \omega_2) = \int \int_{R^2} g(x, y) e^{-i2\pi(\omega_1 x + \omega_2 y)} dx dy. \tag{3}$$

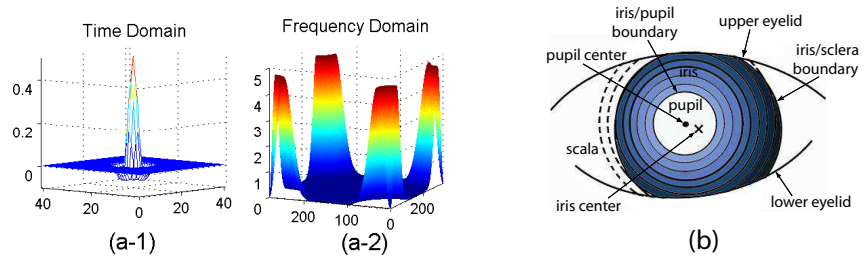

Fig. 3. (a) A Mexican hat wavelet illustrated (a-1) in the space domain, and (a-2) in the frequency domain. (b) Partitioning the iris texture into local regions. Multiple concentric annulus bands with fixed width are constructed and local quality is measured based on the energy in each band.

Then, equation (2) can be re-written in the frequency domain as

$$W(s, \omega_1, \omega_2) = \sqrt{s} F(\omega_1, \omega_2) Phi(s\omega_1, s\omega_2), \tag{4}$$

where W, F and Φ are the Fourier transforms of w, f and ϕ, respectively.

We employ the isotropic Mexican hat wavelet (see Figure 3 (b)), given by:

$$\Phi(s\omega_1, s\omega_2) = -2\pi((s\omega_1)^2 + (s\omega_2)^2) e^{-\frac{1}{2}((s\omega_1)^2 + (s\omega_2)^2)} \tag{5}$$

as the choice for the mother wavelet ϕ. The Mexican hat wavelet is essentially a band pass filter for edge detection at scales s. In addition, the Mexican hat wavelet has two vanishing moments and is, therefore, sensitive to features exhibiting sharp variations (e.g., pits and freckles) and non-linearity (e.g., zigzag collarette, furrows). In order to capture various features at multiple scales, we obtain the product responses given by

$$w^{mul}(s_1, s_2, s_3) = w(s_1) \times w(s_2) \times w(s_3), \tag{6}$$

where s_1, s_2, s_3 are the three scales introduced in Figures 2(II:f-h), namely 0.5, 1.0, 2.0.

To obtain the local quality measure of an iris texture, we partition the region into multiple concentric (at the pupil center) bands with a fixed width until the iris/sclera boundary is reached (see Figure 3(b)). Let T be the total number of bands. The energy E_t of the t-th $(t = 1, 2, ...T)$ band is defined as

$$E_t = \frac{1}{N_t} \sum_{i=1}^{i=N_t} |w_{t,i}^{mul}|^2, \tag{7}$$

where $w_{t,i}^{mul}$ represents the i-th product-based wavelet coefficient in the t-th band, and N_t is the total number of wavelet coefficients in the t-th band. The energy, E_t, is a good indicator of the distinctiveness of the iris features, and hence, a reliable measure of local quality; high values of E_t indicate good quality and vice versa (see Figure 4).

The quality index Q is defined as a weighted average of the band-wise local quality

$$Q = \frac{1}{T} \sum_{t=1}^{T} (m_t \times \log E_t), \tag{8}$$

where T is the total number of bands and m_t is the weight [17]

$$m_t = \exp\{-\|l_t - l_c\|^2/(2q)\}, \tag{9}$$

with l_c denoting the center of the pupil, and l_t denoting the mean radius of the t-th band to l_c. The justification for using weights m_t is that inner iris regions provide more texture [12] and is less occluded by eyelashes compared to outer iris regions.

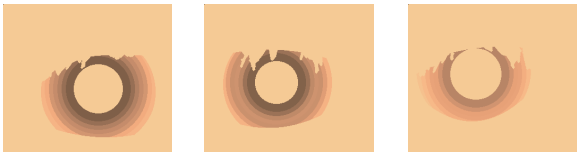

(a) (b) (c)

Fig. 4. The local quality measures based on the energy concentration in the individual bands. The estimated quality indices Q for these three images are 10, 8.6, 6.7, respectively.

(a) (b) (c)

Fig. 5. The normalized iris patterns (top row) associated with Figures 2(I:a-c) and their corresponding normalized quality map (bottom row). The normalization introduces nonlinear distortion when the iris and pupil centers do not coincide.

4 Iris Matching

Before incorporating local quality measures, there are several difficulties in matching two iris images: (i) the iris region may vary due to dilations of the pupil caused by changes in lighting conditions; (ii) the iris size may vary since the capturing distance from the camera is not strictly controlled; and (iii) genuine iris images may have slight rotation due to variability in the acquisition process.

To account for these variations, the Daugman's rubber sheet model [7] is applied to normalize both the iris texture and the local quality measures. Although this nonlinear mapping introduces distortion (Figure 5), it is essential for compensating for pupil dilation and size variability of the iris. Then, Daugman's matching algorithm based on Gabor wavelets is applied to generate the IrisCode for any iris patterns [6]. To measure the similarity of two IrisCodes, X and Y, we compute the Hamming distance, given by

$$HD = \frac{1}{B}\sum_{i=1}^{B} X_i \bigotimes Y_i \ , \tag{10}$$

where X_i and Y_i represent the i-th bit in the sequence X and Y, respectively, and N is the total number of bits in each sequence. The symbol $\bigotimes$ is the "XOR" operator. To account for rotational variability, we shift the template left and right bit-wise (up to 8 bits) to obtain multiple Hamming distances, and then choose the lowest distance.

To incorporate local quality measures into the matching stage, we modify Daugman's matching algorithm by deriving a weighted Hamming distance, given by

$$HD_w = \frac{1}{B}\frac{\sum_{i=1}^{B}\sqrt{E^X_{g(i)} \times E^Y_{g(i)}} \times (X_i \bigotimes Y_i)}{\sum_{i=1}^{B}\sqrt{(E^X_{g(i)} \times E^Y_{g(i)})}} \ , \tag{11}$$

where $g(i)$ is the index of the band that contains the i-th bit of the IrisCode. The symbols $E^X_{g(i)}$ and $E^Y_{g(i)}$ are the associated local quality measures of the $g(i)$-th band in X and Y, respectively. The weighting scheme is such that regions with high quality in both X and Y contribute more to the matching distance compared to regions with poor quality.

5 Experimental Results

Our proposed local quality and the overall quality index Q are derived for two iris databases. The CASIA1.0 database [16] contains 756 greyscale images from 108 different

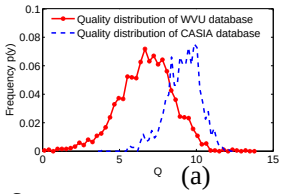

(a)

Accuracy	Iris boundary	Upper eyelid	Lower eyelid
Daugman [6]	98.6%	N/A	N/A
Wildes [11]	99.9%	N/A	N/A
Cui et al. [12]	99.34%	97.35%	93.39%
Proposed	99.47%	98.41%	99.07%

(b)

Fig. 6. (a) Image quality distribution of CASIA1.0 (dotted line) and WVU (solid line) databases. (b) Performance comparison of different segmentation algorithms on CASIA1.0 database.

eyes. The West Virginia University (WVU) Iris Database has a total of 1852 images from 380 different eyes. The number of acquisitions for each eye ranges from 3-6 in this database. The images were captured using an OKI IrisPass-H hand-held device.

Figure 6(a) shows distribution of the overall quality index Q for the two databases. Note the longer left tail of the WVU database, indicating lower quality compared to CASIA1.0. In fact, images in the WVU database were captured without any quality control and were heavily affected by lighting conditions. Further, size of the iris exhibits high variability due to inconsistencies in capture distance during image acquisition.

Since segmentation results on CASIA1.0 are available in the literature [11], we compare them with the performance of our proposed method in Figure 6(b). We can see the proposed method is highly comparable with the others, particularly for lower eyelid detection. Results of Daugman's and Wildes's algorithms were also reported in [11].

Two experiments are conducted to evaluate the proposed quality measures. In the first experiment, we classify images in CASIA1.0 into three quality classes based on Q, namely, Poor (P), Moderate (M), and Good (G). The matching performance for each class is obtained using Daugman's matching algorithm and the corresponding ROC curves are shown in Figure 7 (a). Note that the proposed quality index Q are effective in predicting the matching performance. Higher values of Q indicate better matching performance. In the second experiment, Daugman's matching algorithm was modified by equation (11) and the corresponding ROC curves are obtained. We compare the ERRs of the modified algorithm with those of the Daugman's algorithm. As shown in Figure 7 (b), quality-based matching reduces EERs for all three classes with the greatest improvement on the poor class. Similar experiments were conducted on WVU database (see Figure 7(c-d)). Due to the large size, we classify images in WVU into five classes, namely, Very Poor (VP), Poor (P), Moderate (M), Good (G), and Very Good (VG).

The improvement of matching performance using quality-based matching algorithm is also studied across the entire database, with relative improvements of about 20% (from 1.00% to 0.79%) and 10% (7.28% to 6.55%) in EER observed for the CASIA1.0 and WVU databases, respectively.

6 Summary and Conclusions

In this paper, we study the effects of iris image quality on the matching performance of iris recognition. Two segmentation algorithms are proposed and compared with methods in the literature. Local quality measures based on concentric annulus bands in the iris region are developed using 2D wavelets. Further, we demonstrate that by incorporating the local quality measures as weights for matching distances, the matching performance improves. The capability of predicting the matching performance is also evaluated in terms of the proposed overall quality index Q.

One drawback of the proposed quality measure is its dependency on the segmentation performance, since segmentation itself is affected by poor image quality. In future work, we want to solve this by conducting the two modules in parallel to optimize both.

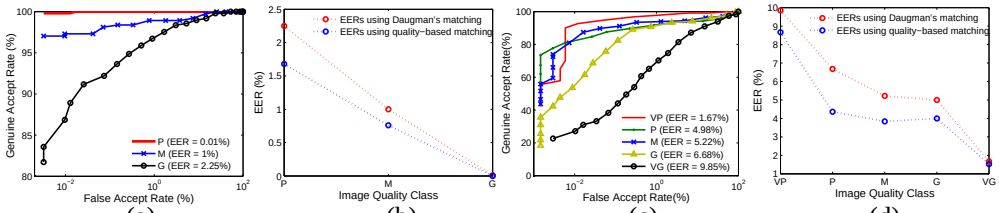

(a) (b) (c) (d)

Fig. 7. Demonstrating the improvement in matching performance using the proposed quality measures on the CASIA1.0 database: (a) ROC curves of the P, M, and G image quality classes. (b) Improvement in the matching performance (in terms of EER) using the proposed quality-based matching algorithm. Similar results on the WVU database: (c) ROC curves of the VP, P, M, G, VG quality classes. (d) Improvement in the matching performance (in terms of EER).

7 Acknowledgements

This work is supported by a contract from the Lockheed-Martin corporation. Thanks to Dr. Arun Ross at West Virginia University and Dr. Yunhong Wang at Chinese Academy of Science for providing the iris databases. Thanks are also due to Mr. Libor Masek for sharing MATLAB code of Daugman's matching algorithm as public resource [18].

References

1. T. Mansfield, G. Kelly, D. Chandler, and J. Kane, "Biometric Product Testing Report," CESG/BWG Biometric Test Programme, National Physical Laboratory, UK, 2001
2. Committee Draft, "Biometric Data Interchange Formats - Part 6: Iris Image Data," *International Organization for Standarization (ISO)*, 2003
3. H. Wang, D. Melick, R. Vollkommer and B. Willins, "Lessons Learned From Iris Trial," *Biometric Consortium Conference*, 2002
4. D. Thomas, "Technical Glitches Do Not Bode Well For ID Cards, Experts Warn," *Computer Weekly*, May, 2004
5. S. King, H. Harrelson and G. Tran, "Testing Iris and Face Recognition in a Personal Identification Application," *Biometric Consortium Conference*, 2002
6. J. Daugman, "Recognizing Persons By Their Iris Patterns", in *Biometric Systems: Technology, Design and Performance Evaluation*, J. Wayman, A.K. Jain, etc. (Eds.), Springer, 2004
7. J. Daugman, "Statistical Richness of Visual Phase Information: Update on Recognizing Persons by Iris Patterns", *Int'l Journal on Computer Vision*, Vol. 45, no. 1, pp. 25-38, 2001
8. G. Zhang and M. Salganicoff, "Method of Measuring the Focus of Close-Up Image of Eyes," *United States Patent, no. 5953440*, 1999
9. L. Ma, T. Tan, Y. Wang and D. Zhang, "Personal Identification Based on Iris Texture Analysis," *IEEE Trans. on Pattern Analysis and Machine Intelligence*, Vol. 25, no. 12, 2003
10. R. Wildes, "Automated Iris Recognition: An Emerging Biometric Technology," *Proc. of the IEEE*, Vol. 85 no. 9, pp. 1348-1363, 1997
11. J. Cui, Y. Wang, etc., "A Fast and Robust Iris Localization Method Based on Texture Segmentation," *SPIE Defense and Security Symposium*, Vol. 5404, pp. 401-408, 2004
12. H. Sung, J. Lim, J. Park and Y. Lee, "Iris Recognition Using Collarette Boundary Localization," *Proc. of the 17th Int'l Conf. on Pattern Recognition*, Vol. 4, pp. 857-860, 2004
13. N. Graham, "Breaking the Visual Stimulus Into Parts," Current Directions in Psychologial Science, Vol. 1, no. 2, pp. 55-61, 1992
14. J. Antoine, L. Demanet, etc., "Application of the 2-D Wavelet Transform to Astrophysical Images," *Physicalia magazine*, Vol. 24, pp. 93-116, 2002
15. C. Burrus, R. Gopinath, and H. Guo, "Introduction to Wavelets and Wavelet Transforms," *Prentice Hall*, New Jersy, 1998
16. Chinese Academy of Sciences - Institute of Automation Iris Database 1.0, available online at: *http://www.sinobiometrics.com*, 2003
17. N. Ratha, R. Bolle, "Fingerprint Image Quality Estimation," IBM RC21622, 1999
18. L. Masek, *http://www.csse.uwa.edu.au/ pk/studentprojects/libor/* , 2003